Quantitative Control over Electrodeposition of Silica Films onto Single-Walled Carbon Nanotube Surfaces†

Mandakini Kanungo,‡ Hugh S. Isaacs,‡ and Stanislaus S. Wong*,‡,§

Condensed Matter Physics and Materials Sciences Department, Brookhaven National Laboratory, Building 480, Upton, New York 11973, and Department of Chemistry, State University of New York at Stony Brook, Stony Brook, New York 11794-3400

Received: December 27, 2006; In Final Form: February 4, 2007

Control over the thickness of a silica coating on single-walled carbon nanotubes (SWNTs) is highly desirable for applications in optics and in biomedicine. Moreover, a silica coating on SWNTs would also aid in avoiding tube−tube contact and bundle formation as well as tube oxidation, a scenario conducive to the use of appropriately functionalized carbon nanotubes as individualized gate dielectric materials in field effect transistors. In this work, we have developed two feasible and reliable means with which to coat SWNTs with various reproducible thicknesses of silica using an electrochemical sol−gel process. In one procedure, a SWNT mat was used as a working electrode for the direct deposition of silica. In the second, nanotubes were dispersed in solution and silica was deposited onto these solubilized nanotubes in the presence of a platinum working electrode. Applying a negative potential results in the condensation of a silica film onto the SWNT surface. The thickness of the silica coating can be controllably altered by varying the potential of the working electrode as well as the concentration of the sol solution. These methodologies have the advantages of ease of use, environmental friendliness, and utilization of relatively mild reaction conditions.

Introduction

The remarkable structure-dependent optical, electronic, and mechanical properties of single-walled carbon nanotubes (SWNTs)[1] have attracted a lot of attention over the past decade due to their potential in applications as varied as molecular electronics, sensing, gas storage, field emission applications, catalyst supports, probes for scanning probe microscopy, and components in high-performance composites.[2−4] Chemical functionalization[5−8] has been used as a route toward rationally tailoring the properties of carbon nanotubes so they can be incorporated into functional devices and architectures. One of the particularly promising and as yet relatively unexplored areas of research involves coating of SWNTs with insulating materials to fabricate nanotube-based devices such as field effect transistors (FETs), single-electron transistors, and gas sensors.[9−11]

In general, the synthesis of a carbon nanotube−insulator heterostructure is important for the use of carbon nanotubes in applications ranging from FET devices to molecular circuits and switches. Specifically, carbon nanotube−silica heterostructure composites are particularly intriguing because of the well-known insulating properties of silica. Indeed, carbon nanotube−silica composites are often critical for applications ranging from electronics and optics to biology. A protective coating of silica can limit the perturbation of the desirable mechanical and electronic properties of nanotubes, while simultaneously providing for a means to functionalize these nanoscale species. In addition, a thin SiO_2/SiO_x coating is optically transparent, and moreover, silica is well-known for its biomolecular compatibility. Furthermore, it is envisaged that the coating of thin, transparent silica on carbon nanotube surfaces would enable their utilization in applications associated with biomedical optics.

Two general strategies have been utilized for silica functionalization of carbon nanotubes. One involves covalent functionalization of silica onto carbon nanotube sidewalls using a range of either silyl or silane derivatives.[12−16] Though covalent functionalization is a robust and a well-controlled process, it may also seriously compromise or otherwise destroy the desirable electronic and optical properties of the carbon nanotubes to a large extent. An alternative strategy has been to coat carbon nanotubes with silica using a noncovalent methodology. A recent theoretical study has shown that a nonbonded, protective layer of silica only weakly perturbs the electronic structure of single walled carbon nanotubes (SWNTs).[17] Therefore, for optimal performance, the existence of a protective layer of silica on the carbon nanotubes should not only enable the retention of desirable electronic, mechanical, and optical properties of carbon nanotubes but also simultaneously and nondestructively functionalize these nanoscale species for a number of diverse applications.

Experimentally, multiwalled carbon nanotubes (MWNTs) coated with silica at room-temperature reveal a higher oxidation resistance and better mechanical properties when compared with heavily processed tubes.[18] An increase in thermal conductivity has been reported for homogeneous MWNT−SiO_2 composites,[19] whereas MWNT/silica xerogel composites have been shown to display enhanced nonlinear optical properties, relative to those of underivatized MWNTs.[20] In addition, MWNT−sol gel composite materials, depending on the nature of the silane precursors used in their fabrication, have been reported to show faster electron-transfer rates and a wide range of favorable capacitance values, thereby providing for enhanced capabilities in the development of novel electrochemical devices using these composites.[21] However, control over the thickness of such a

† Part of the special issue "Richard E. Smalley Memorial Issue".

* To whom correspondence should be addressed. Phone: 631-632-1703; 631-344-3178. E-mail: sswong@notes.cc.sunysb.edu; sswong@bnl.gov.

‡ Brookhaven National Laboratory.

§ State University of New York at Stony Brook.

10.1021/jp068967y CCC: $37.00
Published on Web 04/20/2007

silica coating is contentious but highly desirable. As mentioned, a thin, transparent, biocompatible coating of silica on carbon nanotube surfaces would increase their utilization in optics and in biomedical devices.[22] Moreover, a silica coating onto the carbon nanotubes would also aid in avoiding tube−tube contact and bundle formation as well as tube oxidation, a scenario conducive to the use of appropriately functionalized carbon nanotubes as individualized gate dielectric materials in field effect transistors.[9]

There have been several reports regarding the coating of silica onto both multiwalled nanotubes (MWNTs) and single walled nanotubes (SWNTs) by various methods. Silica coated MWNTs have been prepared using a pulsed laser deposition method wherein the thickness of the layer was varied between 2 and 28 nm.[23,24] SWNTs have been coated with a thin layer of SiO_2 (1 nm) using 3-aminopropyltriethoxysilane as a coupling agent.[25] SWNTs have been derivatized with a fluorine-doped silica layer through a liquid-phase deposition (LPD) process using a silica−H_2SiF_6 solution and a surfactant-stabilized solution of SWNTs.[26,27] In these experiments, Raman, fluorescence, and UV−visible−near-IR studies of silica coated nanotubes suggested the lack of covalent sidewall functionalization occurring on the tubes during the coating process and that importantly, this implied that the coating did not interfere with the electrical properties of the nanotubes. Hollow silica-coated SWNTs and SWNT−silica composite hex nuts have also been synthesized in basic conditions using aqueous sodium silicate.[28,29] Recently, a peptide-mediated route has been reported toward the generation of a silica−SWNT composite in which a multifunctional peptide was initially used to coat, disperse, and suspend SWNTs; this identical peptide was also used to mediate the precipitation of silica and titania onto the carbon nanotube surfaces.[30]

In addition to the above-mentioned techniques, the sol−gel method in particular has been extensively used for the preparation of carbon nanotube−silica composites.[18−21,31,32] The sol−gel technique is well-known in the fabrication of new material composites because of its advantages over conventional processing methodologies, especially for glass-like materials. In the sol−gel process, metal oxide precursors are mixed in the presence of water, alcohol, and either a base or acid catalyst. The molecular-scale reaction tends to form multicomponent materials at much lower temperatures than are normally associated with traditional processing methods. Though a sol−gel process combined with a sintering technique at high temperatures has been developed to yield a SiO_x coating on MWNTs,[18] the same group also reported a room-temperature variation of this protocol, based on the initial creation of positive charges on the MWNT surface by polyelectrolyte adsorption and subsequent deposition of negatively charged SiO_x through a condensation reaction involving tetraethoxysilane (TEOS) in water.[33] A different research team reported a sol−gel method of creating a silica coating on MWNTs,[31] using THF, sodium methoxide, and 3-mercaptopropyltrimethoxysilane.

Though all of these reports have successfully prepared silica coatings on carbon nanotubes, the fundamental problem of actually fine-tuning the thickness of silica on carbon nanotubes remains unresolved. Moreover, published experimental conditions for silica deposition tend to involve the use of harshly acidic or basic conditions, usually necessitate long periods of reaction time, often require a multistep synthesis procedure with the formation of byproducts, and, ultimately, provide for little if any control over the thickness of the as-generated silica coating. In fact, pulsed laser deposition is the only reported method for the quantitative variation of silica thickness of silica with deposition time, but the main disadvantage of this technique is that it requires sophisticated, expensive instrumentation, and lacks the versatility and flexibility of a solution phase-inspired protocol.

In this work, we have developed algorithms with which to coat SWNTs with various reproducible thicknesses of silica by means of the electrochemical sol−gel process. We have used two different experimental protocols. In one procedure, a SWNT mat was used as a working electrode for the direct deposition of silica. In the second procedure, nanotubes were dispersed in solution and silica was deposited on these solubilized nanotubes in the presence of a Pt working electrode. Applying a negative potential results in the condensation of silica onto the carbon nanotube surface. The thickness of the silica coating could be controlled by varying the potential of the working electrode as well as the concentration of the sol solution.

This electrochemical methodology has several advantages. First, the silica appears to be coated on the nanotubes in a noncovalent and therefore nondestructive fashion, as suggested by Raman spectroscopy, X-ray photoelectron spectroscopy (XPS), and UV−visible−near IR spectroscopy data. Second, the procedure is fairly mild and environmentally friendly in that these experiments require a minimum amount of reactants and involve conditions that are neither harshly acidic nor basic. Third, the actual reaction time needed for electrodeposition was only about 5−10 min, as compared with the much longer reaction times associated with other methods. Moreover, all of these experiments were carried out at room temperature under ambient conditions. To the best of our knowledge, this is the first report of the formation of a sol−gel coating of silica on SWNTs through electrodeposition. Furthermore, this is also the first controllable methodology proposed aimed at the fine-tuning of the silica film thickness on carbon nanotube surfaces through a solution-phase methodology involving a rational and systematic variation of reaction parameters.

Experimental Section

Reagents and Materials. Tetramethoxysilane (TMOS, 99%) was purchased from Aldrich Chemicals. High-pressure CO decomposition (HiPco) single walled nanotubes (SWNTs) were obtained from Carbon Nanotechnologies (Rice University, Houston, TX). The working electrode was either a carbon nanotube mat electrode (0.0027 g/cm^2) or a platinum (Pt) foil electrode (1 cm^2). The auxiliary electrode consisted of a platinum foil electrode, whereas the reference electrode was comprised of an Ag/AgCl wire electrode.

Purification of SWNTs. SWNTs were purified using mild oxidizing conditions. In particular, SWNTs were oxidized, under a moist environment, at 180−300 °C in order to oxidize Fe to Fe_2O_3.[34,35] The oxide was subsequently leached by treatment with HCl. It is expected that under these relatively mild oxidizing conditions, purification is not accompanied by extensive functionalization. The suspension of SWNTs in HCl was subsequently filtered through a 0.2 μm polycarbonate filter membrane. After washing repeatedly with distilled, deionized water, a thin self-assembled, free-standing mat consisting of SWNT bundles was peeled from the filtration membrane. The SWNT mats were then dried in a vacuum oven at around 60 °C for 24 h to remove the excess water. We refer to this sample as the "SWNT mat" electrode.

Electrochemical Functionalization. Electrochemical experiments were carried out in a one chamber (three-electrode) cell using a CH potentiostat instrument (Austin, TX). The electrochemical cell consisted of an aqueous solution of TMOS

prepared by mixing 0.1−0.5 mL of TMOS with 2.4 mL of 0.1 M KCl and 2 mL of ethanol. Ethanol acts as a common solvent for the mixing of TMOS and aqueous KCl solution, whereas KCl is used as a supporting electrolyte. Two different experimental procedures were utilized for the deposition of silica onto the carbon nanotube surface and in this work, we have chosen to analyze the results derived from each protocol separately.

Procedure 1. In this protocol, a SWNT mat (0.0027 g) was used as the working electrode. The carbon nanotube mat electrode consisted of a rectangular area measuring 1.0 cm^2. An electrical contact was created by attaching a copper wire to the working electrode through silver epoxy. A Pt foil electrode (area = 1 cm^2) was used as the counter electrode and an Ag/AgCl wire was utilized as the reference electrode. The potential of the working electrode was varied in the range from −500 to −1000 mV vs Ag/AgCl. Electrodeposition was carried out for 5 min using chronoamperometry. Chronoamperometry is a commonly used electrochemical technique in which a constant potential is applied to the working electrode and the current is recorded as a function of time. After silica deposition, the nanotube mat electrode is immersed in water and sonicated in a horn sonicator for 2−3 min in order to debundle the tubes, followed by filtration and centrifugation to remove the excess silica not attached to the nanotubes themselves. The reaction products are then oven-dried at 60−70 °C. In the control experiment, the working electrode (SWNT mat) was placed in the sol solution under identical conditions without applying any potential to the working electrode.

Procedure 2. In the second procedure, SWNTs (0.0027 g) were first ultrasonicated in an aqueous KCl (2.4 mL) and ethanol (2 mL) mixture so as to produce a stable dispersion followed by addition of TMOS (0.1−0.5 mL) and subsequent sonication for a few additional minutes. A Pt foil electrode (1 cm^2) was used as the working electrode. Electrochemical functionalization of silica on SWNTs was carried out mainly using chronoamperometry. Potentials in the range of −700 to −1000 mV were applied to the working electrode for 10 min. Thereafter, the dispersion was filtered, washed repeatedly with water, and oven dried at 60−70 °C. In the corresponding control experiment, the SWNT−sol dispersion was kept in an open circuit potential (i.e., no potential applied) for 10 min followed by filtration and washing.

In this work, silica-coated SWNTs synthesized by procedure 1 will be referred to as Si−SWNT-1, whereas those functionalized by procedure 2 will be named as Si−SWNT-2. Associated control experiments will be denoted as Si−SWNT-ctrl-1 and Si−SWNT-ctrl-2, respectively, in all subsequent discussions.

Characterization of Silica Functionalized SWNTs. Nanotubes were characterized using atomic force microscopy (AFM), scanning electron microscopy (SEM), high-resolution transmission electron microscopy (HRTEM), X-ray photoelectron spectroscopy (XPS), UV−visible spectroscopy (UV−vis), Fourier transform mid- and near-infrared (FTIR) spectroscopy as well as Raman spectroscopy.

Atomic Force Microscopy. AFM height images of purified and silica-coated SWNTs were obtained in Tapping mode in air at resonant frequencies of 50−75 kHz with oscillating amplitudes of 10−100 nm. Samples were dispersed in DMF, spin coated onto a highly oriented pyrolytic graphite (HOPG) substrate, and imaged using conventional Si tips (k = 3−6 N/m) with a Multimode Nanoscope IIIa (Digital Instruments, Santa Barbara, CA). Height measurements of pristine and of the silica-coated nanotubes were taken using the Nanoscope analysis software along a number of different, randomly selected section profiles of the individual tube bundles. The height data for all of the tubes were collected and subsequently averaged over a minimum of 35−40 tubes. We stress that the experiments reported herein were performed on nanotube bundles as opposed to on individualized tubes, because we tried to avoid any possibility of complicated, unforeseen reactivity associated with the nanotube dispersing agent (e.g., the surfactant such as SDS). This paper describes more of a demonstration of principle for coating nanotubes, requiring minimal chemical manipulation of readily available commercial tubes, which tend to occur as bundles. Hence, the methodology herein can be readily generalized to individual tubes, for instance, grown in situ on surfaces.

We also emphasize that the height data recorded for silica-coated tubes accurately reflected only those regions of the tube bundles where an obvious coating was present; we recognize that not all of the tubes possess a continuous surface coating of silica, especially with respect to the thicker coatings. Hence, the actual thickness of the silica film could be obtained by subtracting the average height of the uncoated sections of the tube bundles from the coated regions of tube bundles in the same sample. We should mention that the heights of uncoated tubes were found to be within statistical error of the measured heights of pristine tubes and of tubes subjected to control experimental conditions (i.e., Si−SWNT-ctrl-1 and Si−SWNT-ctrl-2).

Electron Microscopy. HRTEM images were obtained on a JEOL 2010F high-resolution transmission electron microscope, equipped with an Oxford INCA EDS system at an accelerating voltage of 200 kV. An aliquot of an ethanolic solution of the sample was drop dried onto 300 mesh Cu grids (coated with a lacey carbon film), which were subsequently held over a beryllium plate localized inside a homemade sample holder. Samples were also imaged with a field emission SEM (FE-SEM Leo 1550 with EDS capabilities) using accelerating voltages of 5−10 kV at a 2 mm working distance.

X-ray Photoelectron Spectroscopy. For XPS analysis, solid samples were attached onto stainless steel holders using a conductive double sided tape and installed in the vacuum chamber of a XPS surface analysis system (Kratos Analytical Plc model DS800). The chamber was evacuated to a base pressure of about 5×10^{-9} Torr. A hemispherical energy analyzer was used for electron detection. XPS spectra were first collected using a Mg K X-ray source at an 80 eV pass energy and at 0.75 eV steps per sample. Higher-resolution spectra were collected at a pass energy of 10 eV at 0.1 eV steps.

Optical Spectroscopy. FT-mid-IR data were obtained on a Nexus 670 (Thermo Nicolet) equipped with a single reflectance zinc selenide (ZnSe) ATR accessory, a KBr beam splitter, and a DTGS KBr detector. Solid samples were placed onto a ZnSe crystal. Measurements were obtained in absorbance mode using the Smart Performer module. For FT−near IR work, a CaF_2 beam splitter and an InGaAs detector were used. UV−visible spectra were collected at high resolution using a Thermospectronics UV1 with quartz cells maintaining a 10-mm path length. Samples were prepared by sonication in *o*-dichlorobenzene (ODCB). Data were corrected to account for the solvent background.

Raman Spectroscopy. Raman spectra were obtained on solid samples dispersed in ethanol and placed onto a Si wafer. Spectra were obtained on a Renishaw 1000 Raman microspectrometer with excitation from argon ion (514.5 nm), He−Ne (632.8 nm), and diode (780 nm) lasers, respectively. A 50× objective and low laser power density were used for the irradiation of the sample and for signal collection. The laser power was kept sufficiently low to avoid heating of the samples by optic-

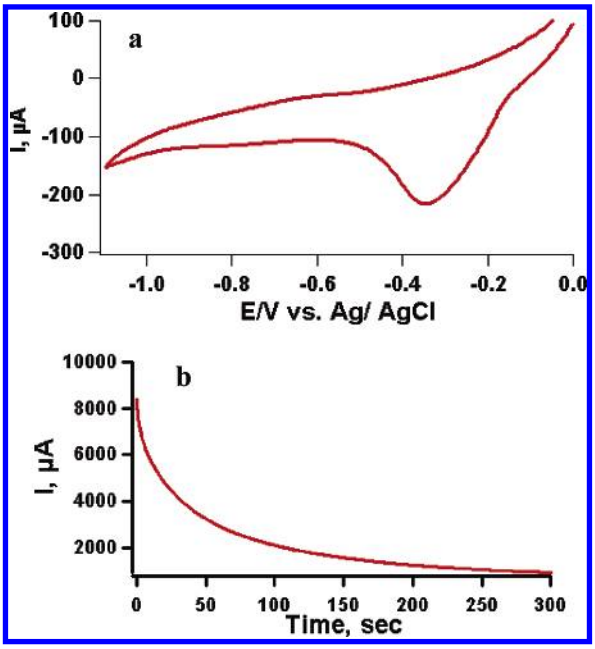

Figure 1. (a) Cyclic voltammogram of a SWNT mat electrode obtained at a scan rate of 10 mV/s. (b) A representative chronoamperometric curve of a SWNT mat electrode in a TMOS sol, showing the response to a potential step from 0 to −700 mV.

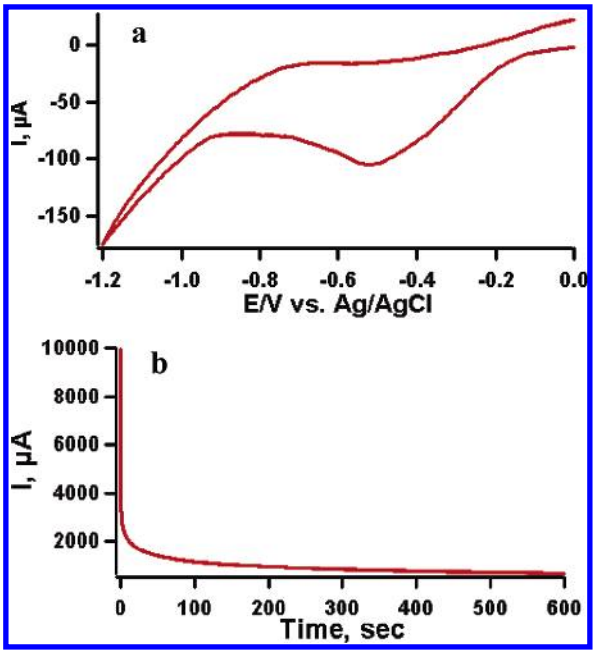

Figure 2. (a) Cyclic voltammogram of a Pt electrode in the presence of a TMOS sol at a scan rate of 10 mV/s. (b) A representative chronoamperometric response of SWNT "electrodes" dispersed in TMOS sol, illustrating the response to a potential step from 0 to −700 mV.

al filtering and/or defocusing of the laser beam at the sample surface. Spectra were collected in the full range of 3000−100 cm^{-1} with a resolution of 1 cm^{-1}.

Results and Discussion

Electrodeposition of Silicate Film on SWNTs. *Procedure 1.* In the electrodeposition process, the application of a constant negative potential to the working electrode causes generation of hydroxide ions at the electrode surface via reduction of water and dissolved oxygen.[36−41] This process is also accompanied by the reduction of protons at the electrode surface. The generation of OH^- increases the local pH around the working electrode. This increased local pH will result in the base-catalyzed hydrolysis and condensation of TMOS with the consequent formation of a silica film of controllable diameter on the electrode surface.[36,37] The production of OH^- depends on the nature of the electrode surface. Details of the mechanism associated with the localized electrode reaction are described in the Supporting Information.

Figure 1a shows the cyclic voltammogram of a carbon nanotube mat electrode in a TMOS sol containing 0.1 mL of TMOS, 2.4 mL of 0.1 M KCl, and 2 mL of ethanolic solution. KCl was used as the supporting electrolyte. It can be observed that, for the carbon nanotube mat electrode, a broad reduction wave occurs at around −350 to −400 mV. This peak has been attributed to the reduction of oxygen to OH^- near the electrode surface, resulting in electrodeposition of the silicate film. We found that applying a potential less negative than −300 mV did not result in any silica deposition on the nanotube surface under aerated conditions. To verify the appropriateness of these conditions, a cyclic voltammogram was recorded in a deaerated TMOS sol saturated with nitrogen. In this case, no reduction wave appears and hence, no silica film was deposited onto the SWNT mat electrode at potentials less negative than −800 mV under nitrogen. Thus, from these observations, silica electrodeposition on the SWNT mat electrode was carried out ambiently at negative potentials ranging from −500 to −1000 mV.

Figure 1b shows the current−time plot recorded at the carbon nanotube mat electrode following a potential step from 0 to −700 mV. Applying a cathodic current density to the electrode surface (−0.1 to −0.3 mA/cm^2) also results in the appearance of silicate films electrodeposited onto the electrode surface. Considering that, after each experiment, SWNT−silica adducts were ultrasonicated and washed repeatedly after centrifugation and filtration, it is reasonable to assume that the silica films on the carbon nanotubes adhered tightly to the carbon nanotube surfaces, as can be seen from SEM and AFM data discussed later in the manuscript. This observation has been attributed to the mediation of oxygenated groups such as alcohol, ketone/aldehyde, carboxylic acid, and epoxy functionalities[35,42] on the SWNT surfaces which can readily bond to the silica film.[36]

Procedure 2. In this case, a Pt foil (1 cm^2) was used as the working electrode with the carbon nanotubes dispersed in the sol. Applying a constant negative potential to the Pt electrode results in the production of OH^- ions and an increase in the local pH near the vicinity of the Pt electrode as well as a corresponding rise in the local pH of the sol itself near the electrode. The silica film can hence be deposited onto the Pt electrode as well as onto the carbon nanotubes dispersed in the sol solution.

Figure 2 shows the cyclic voltammogram of the Pt electrode in the presence of a TMOS sol. For the Pt electrode, the reduction of O_2 to OH^- ions begins at a potential more negative than −500 mV. Indeed, the application of a less negative potential to the Pt electrode does not result in silica deposition either onto the nanotubes or onto the Pt foil itself. This suggests that, for Pt, the electrodeposition process itself commences at a potential more negative than −500 mV. Therefore, in this case, a range of potentials from −700 to −1000 mV could be applied to the Pt working electrode to induce deposition. We noted that a mixed deposit of carbon nanotubes and silica on the Pt foil did not adhere well to the electrode surface with the composite film often flaking off.

From the SEM images shown for these samples, it seemed as if the carbon nanotubes, deposited on the Pt electrode, were

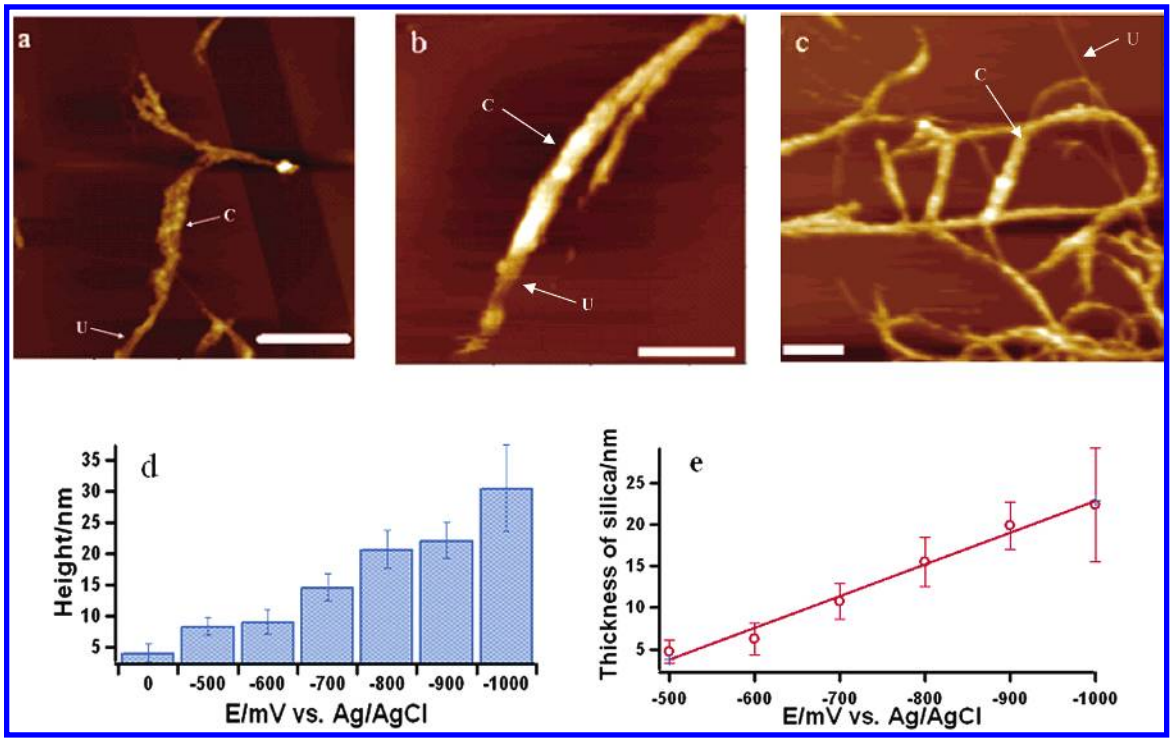

Figure 3. AFM height images of silica-coated carbon nanotubes synthesized by electrochemical silylation using a SWNT mat electrode (Si−SWNT-1) at −500, −700, and −1000 mV (a-c) respectively. The *z* scale is 100 nm for panels a and b and 300 nm for panel c, respectively. The scale bar represents 250, 200, and 250 nm for panels a−c, respectively. Panel d represents the plot of the height of silica-coated SWNTs (Si−SWNT-1) vs applied potential at an open circuit potential of 0, −500, −600, −700, −800, −900, and −1000 mV respectively. Panel e shows the corresponding plot of thickness of the silica film at these various potentials. Letters U and C denote the relatively uncoated and the relatively more heavily coated parts of the nanotube bundles, respectively.

encapsulated by silica (Supporting Information, Figure S1). A similar phenomenon has been observed by other groups while depositing a film of silica onto a platinum electrode by means of the sol−gel technique.[36]

By contrast, carbon nanotubes suspended in solution were covered with a silica film that adhered strongly to the nanotube surface. Hence, in this manuscript, we primarily analyzed silica-coated SWNTs, either dispersed in the sol (Si−SWNT-2) or from a carbon nanotube mat electrode (Si−SWNT-1), by a number of different analytical characterization techniques, including microscopy and spectroscopy.

Summary of Characterization Protocols. Silica-coated nanotubes, synthesized by procedures 1 and 2, were characterized extensively using AFM. AFM height images were recorded for silica-coated nanotubes as a function of applied potential as well as the concentration of the sol solution. Structural characterization was confirmed by electron microscopy (including SEM and HRTEM). Spectroscopic techniques such as XPS, IR, and Raman were also utilized as tools to characterize these adducts.

AFM Characterization. *Functionalized Tubes Synthesized by Procedure 1.* Figure 3a−c shows AFM height images of SiO_x-coated SWNTs (Si−SWNT-1), prepared from deposits isolated from the SWNT mat electrode at −500, −700, and −1000 mV respectively. As seen from the figure, in a prevailing motif we have noted in all of our experiments, silica attaches to the carbon nanotubes as a continuous, roughened coating.

We observe that the silica coating appears to consist of a particulate mass composed of spherical aggregates. This can be attributed to the nature of the base-catalyzed condensation process.[43] In the electrodeposition process, sol condensation occurs first followed by solvent evaporation and subsequent drying, yielding a particulate texture in the resulting film. It was also noted that, with increasing negative potential, the thickness of the film increased. This can be explained by the fact that either the application of an increasing negative potential or a cathodic current density to the working electrode will increase the generation of OH^- ions, which in turn will increase the local pH surrounding the electrode, thereby encouraging and accelerating the electrodeposition process. It is known[44] that the sol−gel process produces deposited films whose morphology is particulate in nature and whose structure is dependent on a variety of factors including but not limited to precursor size, structure, and reactivity, relative rates of condensation and evaporation, and liquid surface tension. Hence, because of the grainy nature of the product of the base-catalyzed sol−gel process, it is not surprising therefore that an increase in film thickness correlated with an increase in surface roughness of the silica coating. That is, thicker coatings, generated at increasing potentials, tended to be more variable from the perspective of both height and roughness measurements. One need only compare the results at −500 vs −700 mV to note the conspicuously more continuous, smoother film (i.e., thinner coating) associated with the run at the less negative potential.

Figure 3d shows a plot of apparent tube height vs applied potential for Si−SWNT-1 tubes. Data were obtained from height measurements of an average of 45−50 nanotubes. Figure 3e shows a plot of the thickness of a silica-coated film on SWNTs vs the applied potential. Average thicknesses of these films were obtained by subtracting the average height of Si−SWNT-ctrl1 from that of Si−SWNT-1 tubes at the same potential.

As previously mentioned, we note that in some cases, there are some portions of the tube, which are not coated with silica, as seen from the figures. This observation can be accounted for by (a) the orientation of the individual tubes in the mat electrode, (b) the entanglement of tubes within the mat electrode,

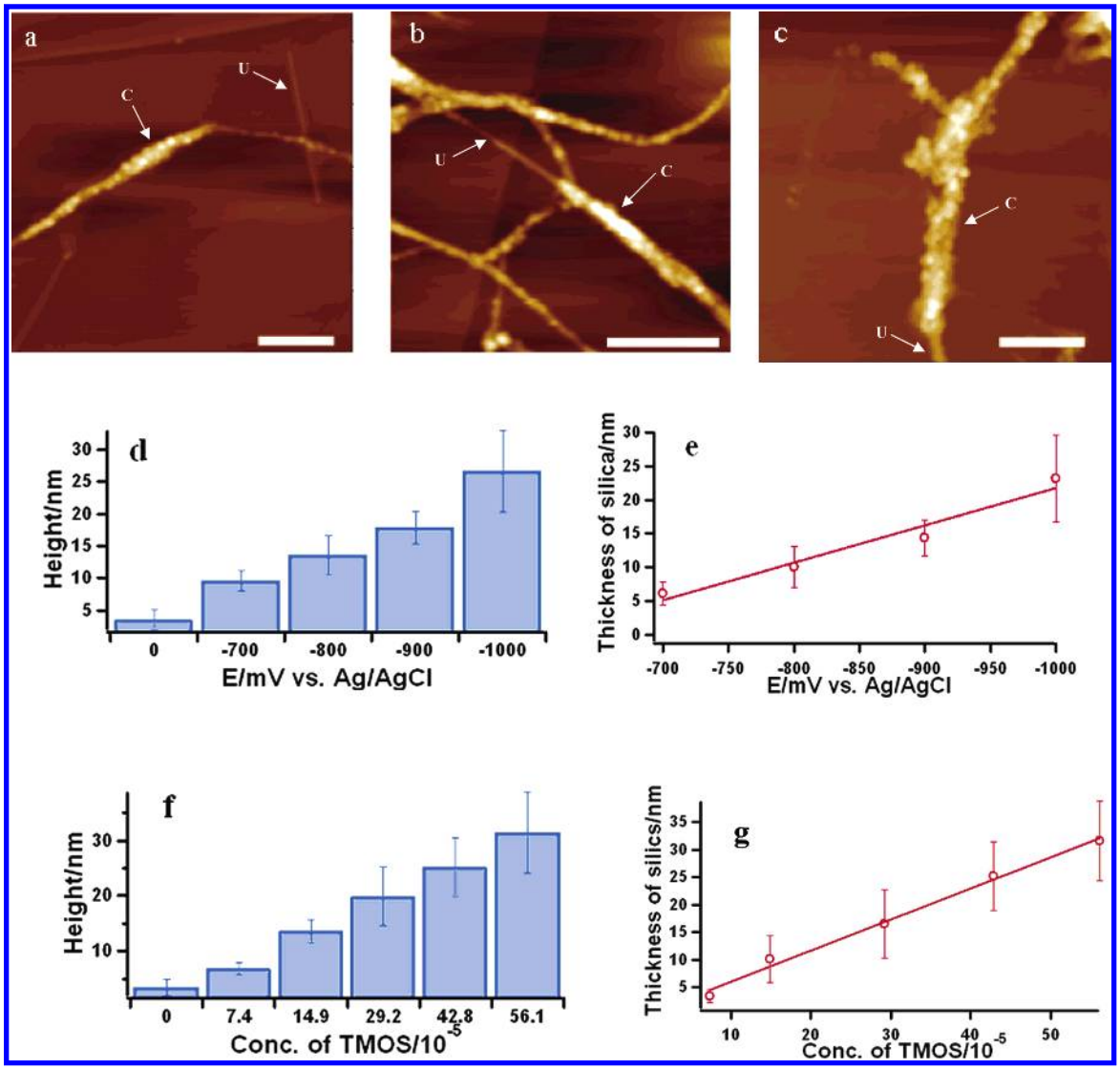

Figure 4. (a−c) AFM height images of silica-coated nanotubes synthesized by electrochemical deposition onto carbon nanotubes dispersed in solution (Si−SWNT-2) at potentials of −800, −900, and −1000 mV respectively. The *z* data scale is 100 nm for panels a and b and 300 nm for panel c. The scale bars for panels a−c are 250, 250, and 200 nm, respectively. Panels d and e represent AFM heights and thicknesses of electrodeposited silica film (Si−SWNT-2) at the negative applied potentials of 0, −700, −800, −900, and −1000 mV, respectively. Panels f and g show the increase in heights and thicknesses (as measured by AFM) of silica-coated nanotubes (Si−SWNT-2) probed as a function of silane concentration in solution (7.4×10^{-5}, 1.49×10^{-4}, 2.92×10^{-4}, 4.28×10^{-4}, and 5.6×10^{-4} M, respectively). Letters U and C denote the relatively uncoated and the relatively more heavily coated parts of the nanotube bundles, respectively.

and (c) the lack of physical exposure of some portions of the tube bundles to the sol itself during the reaction process. Moreover, for thicker coatings of silica, physical cracking was observed in some instances, which could either be partially attributed to sample drying under nonoptimized conditions or to sample breakage occurring during vigorous ultrasonication of the carbon nanotube mat electrode in an effort to isolate individual tubes.

The plot shows a linear increase in the average thickness of the film as a result of an increase in the magnitude of the negative potential ($R^2 = 0.965$). The thickness of the silica films on carbon nanotubes was observed to vary from $\sim 4.4 \pm 1.3$ to 26.6 ± 6.8 nm by tuning the magnitude of the negative potential applied from −500 to −1000 mV with the observed increase in silica found to deposit at a rate of 0.044 nm/mV. This quantitative result highlights the main point of the paper, namely our ability to initiate controllable deposition of silica onto the carbon nanotube surface through a reproducible electrodeposition process.

In all experiments run, more than 80% of the tubes were found to be coated with silica, an observation attributed to the fact that the majority of as-synthesized carbon nanotube mat electrodes were deliberately synthesized with a low enough density (270 μg/ cm^2) of tubes to ensure that the vast majority (i.e., maximal surface area) of individual nanotubes within the mat itself would be exposed to the sol solution. Conversely, in electrodes consisting of denser mats of nanotubes ($\sim$1000 μg/ cm^2), only the outer layers were observed to have been coated with silica.

Functionalized Tubes Synthesized by Procedure 2. Figure 4a−c shows AFM height images of the silica-coated SWNTs that were electrodeposited by dispersing carbon nanotubes in a sol solution in the presence of a Pt foil working electrode at −800, −900, and −1000 mV, respectively. The particulate nature of the silicate film is very clear from the AFM images. In this case, the formation of a silicate film commences at potential values more negative than −500 mV. As mentioned previously, a certain mass of carbon nanotubes was deposited

along with silica onto the Pt foil electrode itself, forming thick white flaky films, with observed silica thicknesses noted to be much larger than those associated with the dispersed carbon nanotubes in solution.

The formation of silica-coated carbon nanotubes in solution (Si−SWNT-2) was attributed to an increase in the local pH of the sol solution in the vicinity of the electrode surface, conditions conducive to gelation of sol onto the carbon nanotube bundles (effectively each individually behaving as an electrode) dispersed in the solution. It should be mentioned that the solution was sonicated rigorously prior to the electrodeposition process to ensure nanotube dispersability and homogeneity in the reaction medium. It was also noted that there is a larger variation in detected heights among the silica-coated nanotubes in these samples, a fact explained by the dependence of the thickness of the coating on the distance of the carbon nanotubes from the working electrode. As the localized increase in pH will be highest near the Pt electrode, therefore, SWNTs in closest proximity to the Pt electrode will possess a thicker silica coating as compared with nanotubes farther away from the electrode.

Figure 4d shows AFM height images of as-prepared silica-coated nanotubes as a function of applied potential. As expected, the apparent heights of the tubes (and incidentally, surface roughnesses of the resulting silica films) increase with increasing negative potential. Figure 4e shows the plot of corresponding thickness of the silica film vs applied potential. The average thickness of the silica film on the carbon nanotube was found to increase linearly with a slope of around 0.055 nm/mV ($R^2 = 0.961$). With this protocol, approximately 65% of carbon nanotubes were found to be coated with silica as compared with 80% noted for nanotubes coated by procedure 1. We have preliminary data that indicate that not only the percentage of tubes coated can be significantly increased but also the thickness variation can be correspondingly decreased by continuous stirring of the reagent solution during electrodeposition. We have also studied the behavior of silica thickness as a function of TMOS concentration (Figure S2). Specifically, the height of silica-coated nanotubes was measured as function of silane concentration in solution (7.4×10^{-5}, 1.49×10^{-4}, 2.92×10^{-4}, 4.28×10^{-4}, and 5.6×10^{-4} M) (Figure 4e) at an applied electrode potential of −800 mV vs the Ag/AgCl electrode. The thickness of the silica coating was found to increase linearly with silane concentration, varying from 3.4 ± 1.2 to 31.5 ± 7.2 nm over the concentration range (Figure 4f). The slope of the corresponding curve, an empirical correlation between the average silica thickness and TMOS concentration, was determined to be 56.4 nm/mM ($R^2 = 0.993$).

Electron Microscopy Characterization. *Functionalized Tubes Synthesized by Procedure 1.* Figure 5a shows the SEM image and the corresponding EDS spectrum of silica-coated SWNTs (Si−SWNT-1), synthesized by electrodeposition at an applied potential of −1000 mV. The EDS spectrum (Figure 5d) shows the presence of a strong Si peak, which is absent in the purified, unfunctionalized SWNTs (PSWNT) as shown in Figure 5f. The oxygen peak of Si−SWNT-1 is also stronger as compared with the EDS spectrum of purified, unfunctionalized SWNTs (Figure 5f), indicating the likely presence of SiO_2 on the SWNT surface.

The presence of a silica coating on Si−SWNT-1 was further confirmed by HRTEM images (Figure 6). Figure 6a shows an HRTEM image and corresponding EDS spectrum (Figure 6d) of purified tubes; it is noteworthy that Si is absent from the EDS spectrum of these cleaned tubes. Figure 6b represents the HRTEM image of carbon nanotubes coated with silica (Si−SWNT-1) at −600 mV. The carbon nanotube structure is clearly intact indicating that it is not destroyed by the electrochemical silylation process. In addition, we observe the presence of a mostly roughened, amorphous coating of silica on the functionalized, small SWNT bundles. The silica film is particulate in nature in agreement with AFM data. The Si peak in the corresponding EDS spectrum (Figure 6e) of those tubes is consistent with the presence of silica on the nanotube surface. The presence of Fe can be attributed to the presence of residual impurities in the sample. Figure 6c shows the HRTEM image of another set of carbon nanotubes coated with silica (Si−SWNT-2) at −700 mV. Again the physical structure of these tubes remained relatively unaffected through this mild nondestructive method of functionalizing carbon nanotubes. The presence of silica was confirmed by the EDS spectrum (Figure 6f) and was noted to be amorphous in nature. We have additional HRTEM results on other tubes/bundles in Figure S3 to further reinforce the validity of our methodology in coating tubes with silica.

It is worth mentioning that the SEM and the corresponding EDS spectrum (e.g., negligible quantities of Si) of the control tubes (Si−SWNT-ctrl-1; Figure S4), in which the SWNT mat electrode was placed in the sol solution for 5 min at an open circuit potential, resemble analogous data for purified, unfunctionalized SWNTs (Figure 5c). We also note that the nanotubes in both the purified and silica-coated samples tend to occur as small bundles measuring 4−10 nm in diameter.

Functionalized Tubes Synthesized by Procedure 2. Figures 5b and 5e show the SEM image and the corresponding EDS spectrum of SWNTs (Si−SWNT-2), electrodeposited at a potential of −1000 mV. The presence of a strong Si peak combined with an oxygen peak indicates the likelihood of silica on the surfaces of these tubes. The presence of silica on the functionalized carbon nanotubes was further confirmed by HRTEM images showing the presence of an amorphous but roughened coating on the SWNT surface (Figure 6c). Conversely, as mentioned previously, the control experiment does not show the presence of a Si peak in the EDS spectrum.

Spectroscopy. *Interpretation by XPS Spectra.* XPS was used to reveal the surface state composition of SWNTs before and after silica coating. High-resolution data for samples analyzed are presented in Figures S5−S7. The XPS atomic concentrations of purified, air-oxidized SWNTs (C = 81.10%, O = 13.91%, Si = 1.29%) are evidence for the presence of carbon and oxygen with a trace quantity of Si in the precursor tubes. The presence of Si, fluorine, sulfur, and chloride can be assigned to intrinsic impurities associated with as-purchased nanotubes. The presence of oxygen, however, can be attributed to extant surface oxides on the carbon nanotubes.

Si−SWNT-1 synthesized at a potential of −1000 mV (C = 43.72%, O = 40.27%, Si = 15.43%) suggests that the functionalization process had a direct correlation with the amount of Si observed. The atomic concentration of oxygen increased as well, corroborating the possible formation of SiO_2. Conversely, the XPS atomic concentrations measured of Si−SWNT-ctrl-1 (C = 86.97%, O = 9.71%, Si = 1.53%) show the composition of carbon, oxygen, and silicon to be approximately the same as that of purified SWNTs.

The high-resolution C 1s spectra of purified, air-oxidized SWNTs reveal peaks in the range of 283−292 eV. The main peak (284.59 eV) has been attributed to the C 1s signal of graphitic carbon, whereas other peaks have been assigned to −C−OH (286.1 eV), −C═O (287.5 eV), and −COOH

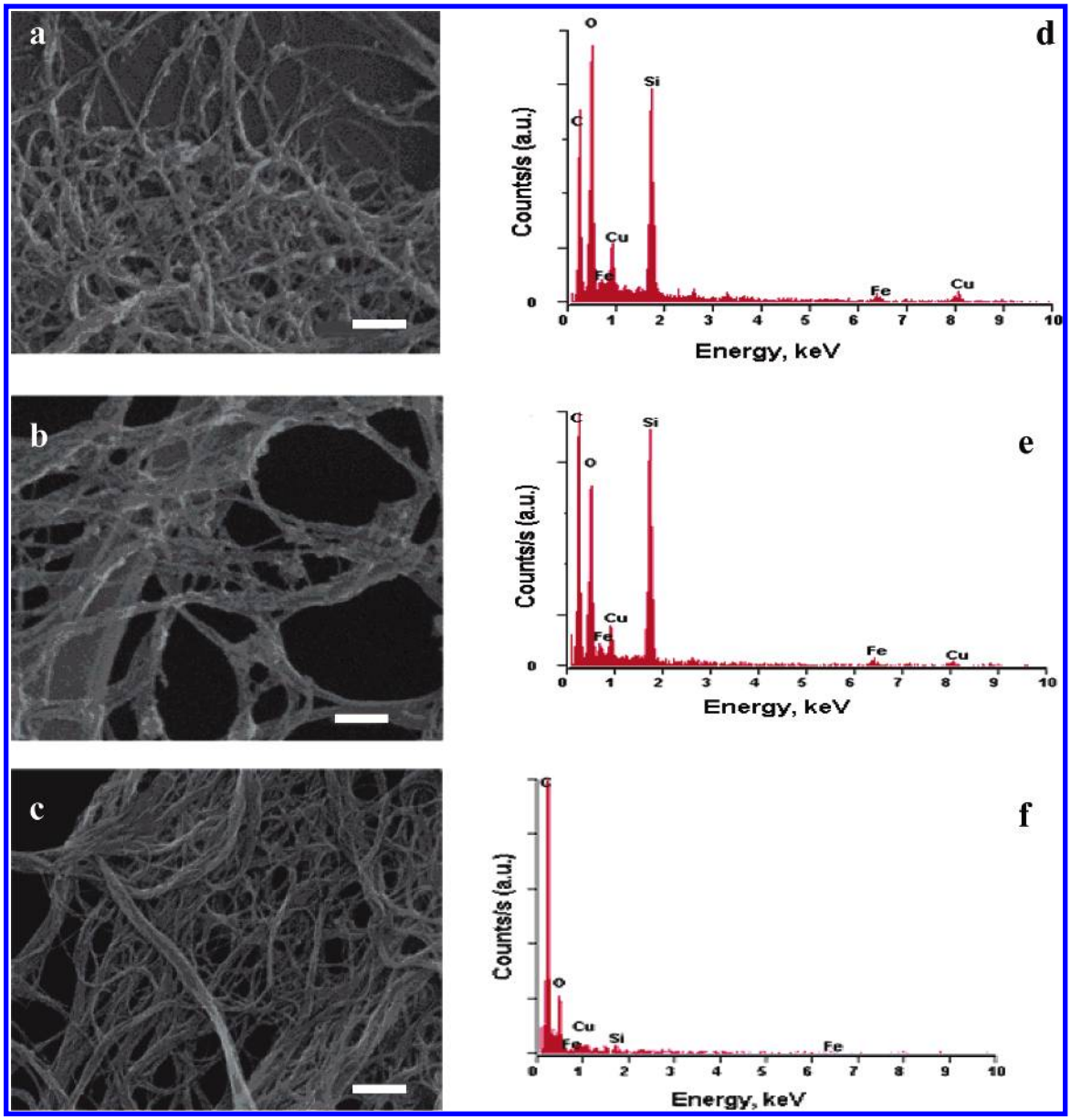

Figure 5. SEM images and corresponding EDS spectra (d−f) of (a) silica-coated carbon nanotubes prepared from a carbon nanotube mat electrode (Si−SWNT-1) and of (b) nanotubes, electrodeposited with silica, from solution (Si−SWNT-2). (c) Purified, air-oxidized SWNTs. The scale bar is 100 nm. In the EDS spectra, the presence of Fe can be attributed to remnant catalytic impurities, while the Cu signal can be assigned to the grid.

(289.13 eV) groups, respectively, indicating the presence of oxygenated functional groups on the carbon nanotube surface due to air oxidation.[45,46] From the C 1s and O 1s spectra, the purified carbon nanotubes were determined to possess approximately 30% functional group derivatization with the presence of −OH, −COOH, and −C═O groups, respectively.

The high-resolution C 1s peaks of Si−SWNT-1 (284.56, 286.50, 288.00, and 289.01 eV) were found to minimally shift with respect to those of purified, air-oxidized SWNTs, suggestive of the lack of covalent functionalization of the SWNT surface.[27] The high-resolution Si 2p spectrum shows a peak located at 104.11 eV, which can be attributed to the SiO_2 signal, resulting from a siloxane network (Si−O−Si) of bonds originating from the condensation of silane molecules. The apparent absence of either Si−O−C or Si−C bonding suggests that the silica is attaching to the SWNT surface through van der Waals interactions. Atomic concentrations (%) of the elements and the relative percentages of these elements in the various samples are given in Table 1.

UV−Visible−Near IR Spectroscopy. Figure 7a shows the UV−visible spectra of purified, air-oxidized SWNTs, Si−SWNT-1, Si− SWNT-2, and pristine SWNTs. The spike-like features observed in the UV−visible spectra of the pristine SWNTs can be attributed to optical transitions originating between van Hove singularities of the local electronic density of states of the nanotubes. In the UV−visible spectra, distinctive peaks corresponding to the second transition of semiconducting SWNTs (550−900 nm) and the first transition of metallic tubes (400−600 nm) can be observed for purified HiPco tubes as well as for the Si−SWNT-ctrl-1 and Si−SWNT-ctrl-2 control tubes, as reported in the literature.[7,47] These spike-like features are retained in the signal due to the purified, air-oxidized samples, suggesting that mild air oxidation neither destroys nor adversely affects the electronic properties of tubes, an assertion supported by our Raman data.

On the other hand, features in the UV−visible spectra of silica-coated tubes are diminished to a certain extent, and these are not as clearly distinctive as those of uncoated SWNTs. It

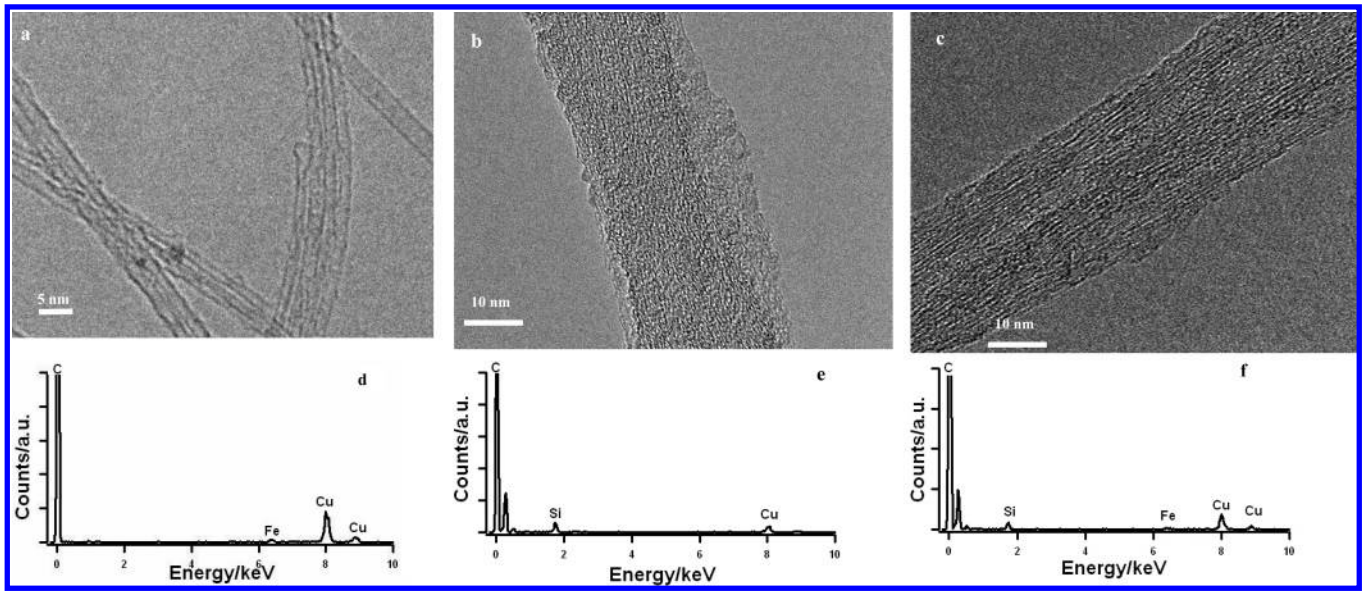

Figure 6. (a) HRTEM image of purified tubes. (b) HRTEM image of Si−SWNT-1 electrodeposited at −600 mV. (c) HRTEM image of Si−SWNT-2 electrodeposited at −700 mV. Scale bars for panels a−c are 5, 10, and 10 nm respectively. Panels d−f show the EDS spectra of purified tubes, Si−SWNT-1, and Si−SWNT-2 tubes, respectively. The presence of Fe can be attributed to remnant catalytic impurities, while the Cu signal can be assigned to the grid.

TABLE 1: XPS Data of Atomic Concentrations (%) of Elements on the Surfaces of Purified, Silanized and Control Nanotube Samples

sample	C	N	O	F	Si	S	Cl	Fe
purified SWNTs	81.1	0.73	13.9	1.70	1.29	0.89	0.38	
control sample (SWNT-Ctrl-1)	87.0		9.71	1.25	1.53			0.55
silanized SWNTs (Si−SWNT-1)	43.7		40.3	0.57	15.4			

must be stressed, that even though there is a minor attenuation, we have not found a complete loss of the intensity of the observed transitions which would have been indicative of covalent sidewall functionalization. This piece of evidence further supports the noncovalent nature of the chemical interaction between SWNTs and SiO_2.[48]

Figure 7b shows the FT−mid-IR spectra of silica-coated nanotubes prepared by procedures 1 and 2 (Si−SWNT-1 and Si−SWNT-2) under conditions of electrodeposition at −1000 mV. The mid-IR spectrum of these functionalized tubes shows peaks located at 1074 and 790 cm^{-1}, suggestive of the presence of a Si−O−Si bonding network on the carbon nanotubes. A shoulder at 920−970 cm^{-1} is consistent either with Si−O stretching of the Si−O-aromatic group or with the benzene ring of the carbon nanotubes. Therefore, the presence of all of the above-mentioned spectroscopic signals is consistent with a silica coating on the carbon nanotube surface.

FT−near-IR measurements (Figure 7c) of the pristine, control, and air-oxidized nanotubes show peaks in the ∼6000−7500 and ∼8000−9500 cm^{-1} regions, corresponding to transitions between the first and second set of van Hove singularities in the semiconducting tubes, respectively.[7,49] As a general comment, we do not observe sharp, discrete peaks, characteristic of individualized tubes, in our optical data, as we have been working with bundles of tubes in these experiments; our results are in fact consistent with data previously observed by independent groups on nanotube bundles.[50,51] Nonetheless, it is evident that the transitions of the functionalized tubes are broadened and shifted from those of the purified tubes, likely due to a change in tube bundling characteristics upon reaction and to the presence of a silica coating on the tubes.[52] The apparent relative enhancement of the absorbance ratio of metallic (>11 000 cm^{-1} region) vs semiconducting tubes for the functionalized adducts as compared with their nonderivatized adducts has been previously observed and is consistent with a noticeable increase in tube−tube interaction, aggregation, and bundling effects as opposed to any true electronic selectivity associated with the current reaction.[51]

Raman Spectroscopy Characterization. Resonance Raman spectroscopy is a very sensitive probe in determining the structural and electronic properties of carbon nanotubes.[53−55] The position and intensity of the bands in Raman spectra are strongly dependent upon the laser excitation energy used because different nanotubes with different diameters and chirality (and hence electronic characteristics be they metallic or semiconducting) are in resonance at different excitation energies.

The SWNT Raman spectrum is determined by three main band regions: the radial breathing mode (RBM) (100−350 cm^{-1}), the tangential mode (G-band) (1500−1600 cm^{-1}) and the disorder D mode (1280−1320 cm^{-1}).[54,55] The RBM features correspond to coherent vibrations of the carbon atoms in the radial direction and are strongly dependent on the diameter of the tubes. By contrast, the tangential mode is weakly dependent on the diameter of the nanotubes but shows distinctive behavior modes for metallic and semiconducting tubes. It is known that the semiconducting nanotubes have narrow Lorentzians in this region whereas metallic nanotubes are characterized by a high-frequency Lorentzian coupled to broad low-energy Breit−Wigner−Fano (BWF) tails.[56] The Fano component in metallic SWNTs essentially arises from the coupling of discrete phonons to an electronic continuum.[57] The intensity of the defect or disorder band is a measure of the conversion of sp^2 to sp^3-hybridized carbon in the intrinsic structural frame network of SWNTs. A sizable increase in the ratio of the disorder D mode to G mode intensity after chemical treatment implies disruption of the electronic band structure of derivatized carbon nanotubes and is a diagnostic for potentially destructive, covalent chemical functionalization of nanotube sidewalls.[5,58−60]

In the present study, we focus on the radial breathing modes and the disorder modes observed in the Raman spectra of our samples. In addition, we also explicitly divide our discussion

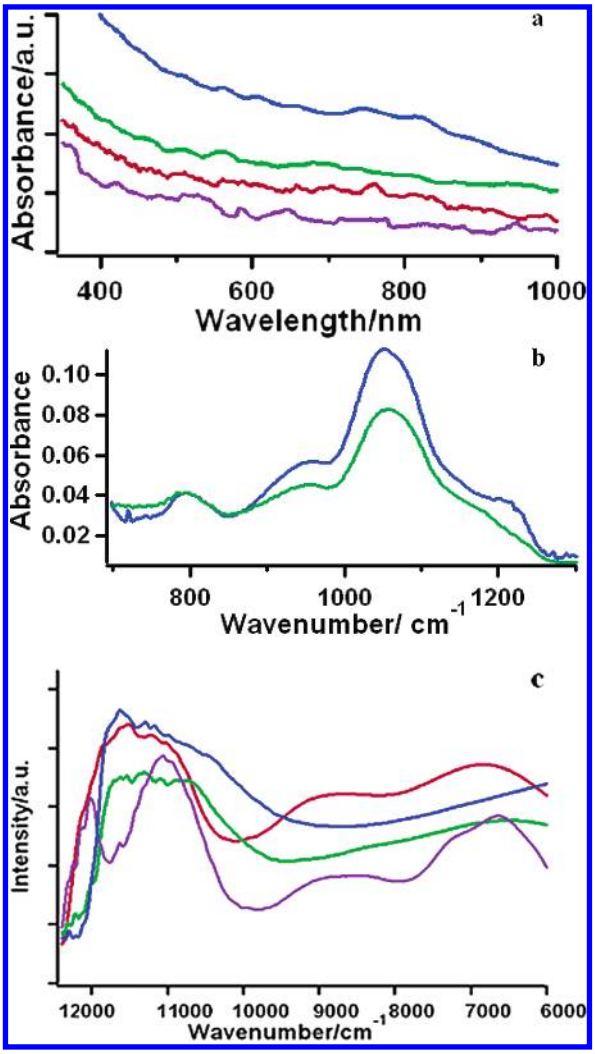

Figure 7. Purified SWNTs (red); Si−SWNT-1 electrodeposited at −1000 mV (blue); Si−SWNT-2 electrodeposited at −1000 mV (green); and pristine samples (purple). (a) UV−vis spectra. (b) FT−mid-IR spectra. (c) FT−near IR spectra of nanotube samples.

for RBMs into two parts: (1) a comparison between air-oxidized nanotubes and their pristine counterparts as well as (2) a comparison between silica-functionalized nanotubes and air-oxidized nanotubes from whence they were derived.

The radial breathing mode (RBM) frequency, ω_{RBM}, is inversely proportional to the diameter of the nanotubes (d_t) presented empirically by eq 1

$$\omega_{RBM} = C_1/d_t + C_2 \quad (1)$$

with $C_1 = 223.5$ (nm cm^{-1}) and $C_2 = 12.5$ cm^{-1}, based on studies of individual HiPco nanotubes.[61,62] RBM bands are also sensitive to the degree of aggregation and bundling of the carbon nanotubes themselves. It has been shown by previous studies that the 266 cm^{-1} peak at 514.5 and 780 nm excitation and 218 cm^{-1} peak at 632.8 nm excitation wavelength can provide information about the extent of aggregation.[63−65] All spectra analyzed were normalized at a specific RBM feature. This normalization at specific RBM features allows for the evaluation of the relative intensities of different, varyingly reacted nanotubes present in the different samples. It should be noted that there was no net change in the overall population of nanotubes during either the oxidation or electrochemical functionalization steps. Hence, we did not expect a loss of nanotubes during these processes.

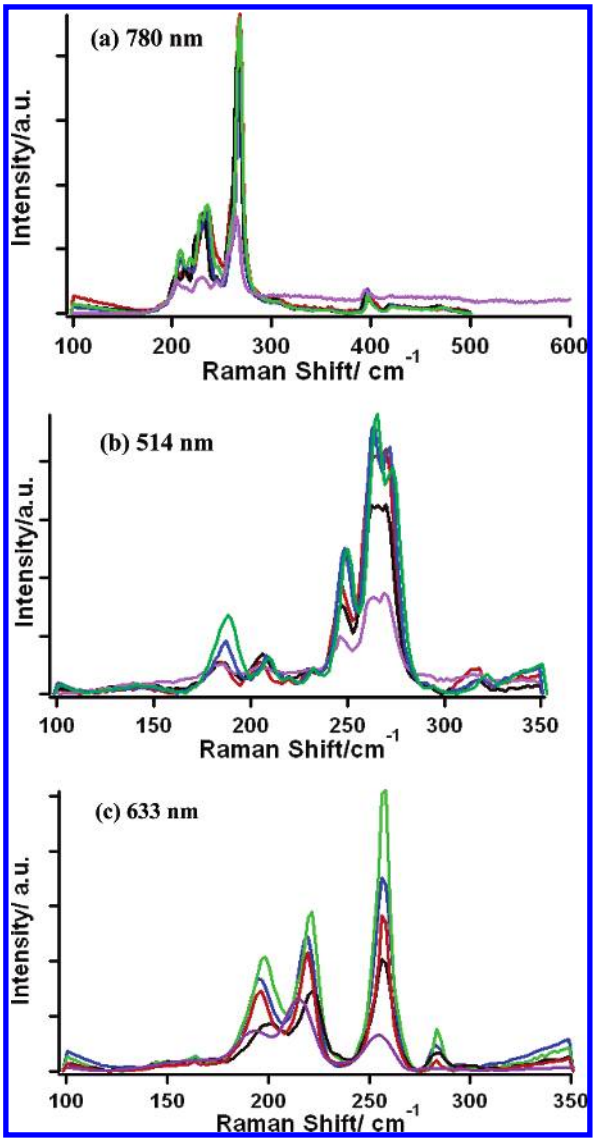

Figure 8. Raman spectra (RBM region) of pristine HiPco SWNTs (purple), air oxidized nanotubes (red), Si−SWNT-1 (blue), Si−SWNT-2 (green), and Si−SWNT-crtl-1 (black). (a) Excitation at 780 nm with normalization with respect to RBM feature at 394 cm^{-1}, (b) Excitation at 514.5 nm wavelength with normalization with respect to 231 cm^{-1} (c) Excitation at 632.8 nm wavelength with normalization with respect to the RBM feature at 164 cm^{-1}.

Comparison of RBM Features between Air-Oxidized and Pristine HiPco Tubes. As described earlier, air oxidized nanotubes are generated under a relatively mild oxidation process and the process itself is considered to be a relatively nondestructive means of nanotube purification.[35] That is, unlike the ozonolysis reaction which substantially disrupts the electronic properties of functionalized nanotubes, air oxidation is not expected to severely disrupt the electronic properties of carbon nanotubes, which is consistent with what we have observed from our own results in the D band region. Nevertheless, because of effects such as hydrogen bonding, the bundling/aggregation effect of nanotubes will likely influence the shape of the RBM bands of air-oxidized tubes at different excitation wavelengths.

Figure 8a depicts the RBM modes of Raman spectra at 780 nm excitation. At this laser wavelength, the excitation is primarily resonant with the $\upsilon 2 \rightarrow$ c2 transitions of semiconducting nanotubes. The purple line represents the signal due to pristine nanotubes, whereas data in red are associated with their

air-oxidized counterparts. The RBM feature at 233 cm^{-1} corresponds to 1.01 nm diameter tubes and has been assigned to (11, 3) semiconducting nanotubes, whereas the feature at 266 cm^{-1} has been assigned to either (10, 2) or (11, 0) nanotubes corresponding to nanotubes possessing a diameter of 0.88 nm.[63] A key finding is the considerable increase noted in the intensity of the RBM feature at 266 cm^{-1} for the air-oxidized nanotubes as compared with their pristine counterparts, an observation consistent with an increase in aggregation or bundling of air-oxidized carbon nanotubes as compared with their pristine counterpart.[63,64] We attribute this to an increase in intertube interactions for air-oxidized tubes because of an increased propensity for hydrogen bonding among the tubes and tube bundles.

The same trend is also observed at the excitation wavelength of 514.5 cm^{-1} (Figure 8b), which brings smaller-diameter metallic as well as larger-diameter semiconducting tubes into resonance.[66−68] The RBM features at 205, 232, and 248 cm^{-1} have been assigned to (9, 8), (11, 3), and (12, 0) nanotubes corresponding to tubes measuring 1.17, 1.01, and 0.95 nm in diameter, respectively. The feature at 187 cm^{-1} has been designated by a (13, 5) semiconducting nanotube possessing a diameter of 1.28 nm. Prominent RBM features are localized at 264 and 272 cm^{-1}, which can be assigned to (7, 6) and (9, 3) nanotubes with diameters of 0.90 and 0.86 nm, respectively. As we observed previously upon excitation at 780 nm, there is a distinctive increase in the peak intensity at both 264 cm^{-1} and 272 cm^{-1} in the spectrum for air-oxidized nanotubes as compared with their pristine counterparts, which can be ascribed to an increase in the aggregation state of air-oxidized carbon nanotubes as compared with their pristine analogues.

Results upon excitation at 633 nm, which probes both the metallic and semiconducting tubes, are shown in Figure 8c.[65,69] RBM features at 194 and 218 cm^{-1} have been assigned to the (9, 9) and (12, 3) metallic tubes corresponding to diameters of 1.24 and 1.09 nm, respectively. A set of peaks localized at 256 nm and at 283 nm have been assigned to (9, 4) and (7, 5) nanotubes, respectively, with diameters ranging from 0.83 to 0.92 nm. The peak at 218 cm^{-1} has been previously attributed to nanotube bundling and was found, as expected, to be higher in intensity for air-oxidized nanotubes as compared with their pristine counterparts,[65] consistent with the idea of aggregation of the purified tubes.

Comparison of RBM Features between Air-Oxidized and Silica-Functionalized Nanotubes. Returning to Figure 8a, with RBM data at 780 nm excitation, the air oxidized nanotubes, Si−SWNT-1, Si−SWNT-2, and Si−SWNT-ctrl-1 samples are represented by the red, blue, green, and black curves, respectively. The peak positions of the RBM features of the silica-functionalized nanotubes are similar to those of the air-oxidized nanotubes previously discussed. It is noteworthy that in all of our data, we do not observe any conclusive evidence for either diameter or electronic structure selectivity in the functionalization reaction. We attribute this effect to the fact that in the condensation reaction reported herein, silica simply coats all nanotubes and nanotube bundles non-discriminately. The intensities of the RBM feature at 266 cm^{-1} for the Si−SWNT-1 and Si−SWNT-ctrl-1 samples are essentially identical to those of air-oxidized nanotubes, suggesting that silica merely coated bundles of loosely connected carbon nanotubes within the mat electrode. Aggregation was more pronounced in the Si−SWNT-2 sample, implying a more effective bundling regimen during the functionalization reaction when the nanotubes were suspended and dispersed in solution. Similar trends were noted

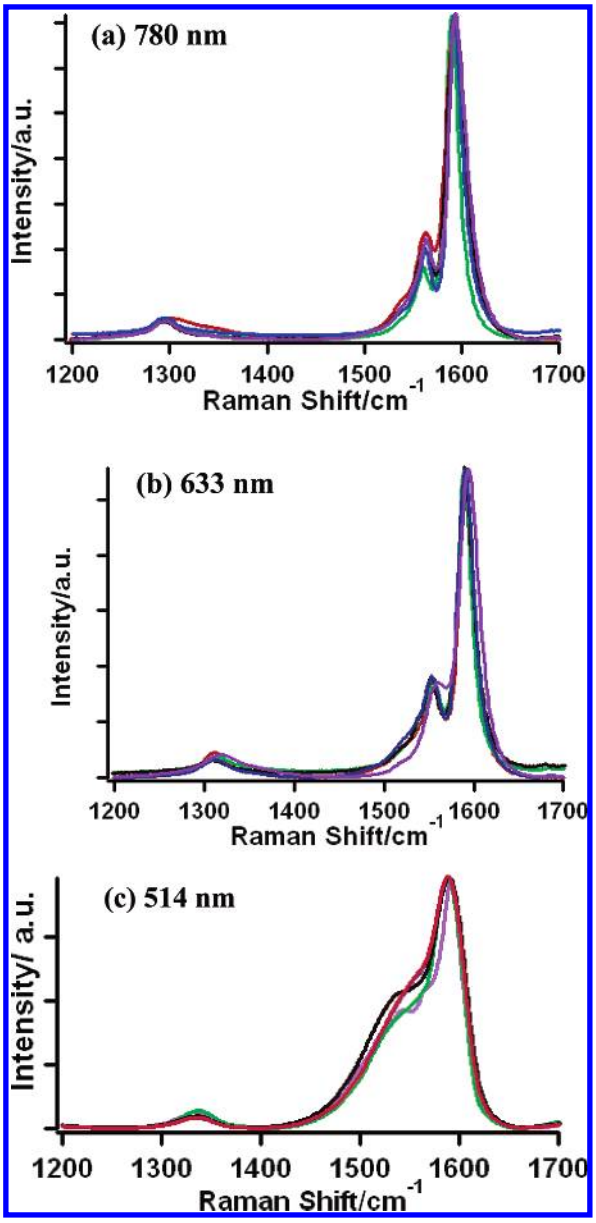

Figure 9. Raman spectra of tangential and disorder mode regions of pristine HiPco SWNTs (purple), purified air oxidized nanotubes (red), Si−SWNT (blue), Si−SWNT-2 (green), and Si−SWNT-ctrl-1 (black). Excitation at (a) 780, (b) 632.8, and (c) 514.5 nm wavelengths, respectively. Spectra were normalized with respect to the G^+ feature.

at both excitation wavelengths of 514 and 633 nm. The corresponding intensities of peaks at 266 and 218 cm^{-1}, respectively, were considerably enhanced, especially with respect to identical peaks of the pristine tubes, for both Si−SWNT-1 and Si−SWNT-2 samples, suggestive of significant silica coating on and therefore, aggregation of bundles of carbon nanotubes upon functionalization.

D and G Band Analysis. Figure 9a depicts the Raman spectra of air-oxidized (red) and pristine nanotubes (purple) in the region of 1200−1700 cm^{-1} upon excitation at 780 nm. We note that unlike for tubes subjected to ozonolysis[70] wherein it is expected that potentially damaging covalent functionalization occurs upon chemical treatment, in the current study, we do not observe a significant change in the intensity of the D band upon air oxidation. This conclusion supports our inherent assumption that air oxidation represents a mild protocol for nanotube purification without significant destruction of the electronic band structure of the processed nanotubes. Furthermore, the intensity of the D

band also remains relatively unchanged (i.e., unaffected) for silica-functionalized tubes (Si−SWNT-1 and Si−SWNT-2) as well as for the control samples. This piece of evidence, taken in context with our other results, provides strong corroboration that the silica electrodeposition reaction is a noncovalent one; the lack of a strong D band signal suggests the absence of covalent functionalization of the carbon nanotube sidewalls. In other words, the electronic structure of the sidewalls is barely affected by the electrodeposition reaction. Our work therefore provides experimental justification for the theoretical assertion that a nonbonded, protective layer of silica only weakly perturbs the electronic structure of SWNTs.[17] Data at 632.8 nm (Figure 9b) are consistent with this picture and show similar behavior, i.e., minimal alteration in the D band intensity for functionalized as compared with pristine samples.

Figure 9c shows the Raman spectra at 514.5 nm excitation wavelength. At 514.5 nm, the pristine nanotubes have a large Fano component since mostly metallic tubes are brought into resonance at this wavelength. There was some broadening of the Fano line shape as one progressed from pristine to air-oxidized to silica-derivatized tubes; it has been reported that Fano features are sensitive to changes in the state of aggregation upon functionalization.[71] The most critical observation remains though that no significant change in the D band intensity was observed for air-oxidized tubes as compared with their pristine counterparts, implying the electronically nondestructive nature of our electrodeposition protocols.

Comparison between Two Methods of Electrodeposition. We have demonstrated by two different procedures that SWNTs can be coated with a controllable thickness of silica film, depending on the magnitude of the potential, precursor silane concentration, and time of deposition. There seem to be a number of advantages and relatively minor accompanying disadvantages associated with each procedure.

In the first procedure, SWNT mat electrodes were reproducibly prepared using a known density of SWNTs in each case. The main advantage of this methodology is that SWNTs could be directly used as the working electrode for silica deposition. An additional advantage is that the reduction process involving oxygen appeared around −300 mV, occurring at a much less negative value as compared with what would have been expected using either a Pt, glassy carbon, or ITO electrode.[36,37] Third, the thickness of this coating could be carefully fine-tuned by judicious variation of a wide range of potentials and concentrations of the sol solution.

The carbon nanotube mat electrode can be visualized as a porous entity in which carbon nanotubes are entangled with each other within a gap-filled mesh; not surprisingly, these types of mat electrodes are mechanically fragile. When the carbon nanotube mat electrode is thin, either individual nanotubes or small bundles of the nanotube will have maximal exposure to the sol solution for silica deposition to occur on the largest number of SWNTs. Nonetheless, our methodology is also conducive to the formation of silica on more robust, thicker free-standing carbon nanotube films. However, in these latter systems, produced from thicker densities of nanotubes measuring 1000 μg/cm^2, we have tended to observe that only the outermost layers of nanotubes are coated with silica and that to functionalize the interior of the nanotube would require potentially destructive sonication (and accompanying cracking) of the film.

In the second procedure, nanotubes have been dispersed in a sol solution, and electrodeposition was carried out using a platinum working electrode. As we have indicated previously, a localized pH change in the vicinity of the Pt electrode will result in the base-catalyzed condensation of the sol and subsequent deposition of silica onto the carbon nanotube surface. We recognize that this is an indirect method for coating carbon nanotubes with silica in that the thickness of the silica coating will depend on the physical distance of the dispersed carbon nanotubes themselves from the working electrode. However, we have overcome this possible limitation by minimizing and thereby optimizing the amount of sol solution and precursor silane concentrations used, as well as by rapid and continuous stirring during the electrodeposition process to ensure a more homogeneous coating of silica on the carbon nanotubes.

Conclusions

In summary, we have demonstrated for the first time that carbon nanotubes can be coated with a stable and reproducible film of controllable thickness using a reasonably simplistic protocol. The methodology developed has several advantages over other previously reported techniques in that the thickness of the resultant silica film can be controlled rather easily by rationally varying reaction parameters such as potential and current, as well as reaction time and sol concentration. This level of control allows for these functionalized tubes to be used in a variety of electronics and optics applications.

We have demonstrated by Raman, UV−vis−near-IR, XPS, and other spectroscopic techniques that silica is not covalently attached to the carbon nanotube, but is rather noncovalently bound to the tubes through van der Waals interactions. This is a significant finding because covalent attachment of functional moieties onto carbon nanotube surfaces may destroy their desirable electronic properties. More generally, this electrochemical technique is mild, nondestructive, and environmentally friendly in that it requires minimal amounts of reactants and reaction steps. Moreover, it can operate under either aqueous or mildly ethanolic reaction conditions, without the need for either harsh acidic or basic conditions, and also, this procedure can be carried out at ambient temperature and pressure conditions under relatively rapid reaction times. This methodology is important for a number of practical reasons including (a) the ability to biocompatibilize carbon nanotubes through the silica coating, rendering these materials useful for a wide range of biological applications, (b) the generation of carbon nanotubes with high resistance to oxidation, and (c) the generalization of this technique to other oxide materials thereby creating the potential for functional nanocomposites. We are currently working on methods to optimize the quality of silica film deposition.

Acknowledgment. This article is dedicated to the memory of Professor Richard E. Smalley. Research (facilities, personnel) was supported in part by the U.S. Department of Energy Office of Basic Energy Sciences under Contract DE-AC02-98CH10886. Acknowledgment is also made to the National Science Foundation for a CAREER award (DMR-0348239), and the donors of the Petroleum Research Fund, administered by the American Chemical Society, for PI support of this research. S.S.W. is an Alfred P. Sloan Research Fellow (2006−2008). Dr. Yuanbing Mao, Mr. Hongjun Zhou, and Professor J. Huang are thanked for their assistance with the HRTEM results.

Supporting Information Available: (i) Description of mechanism of base-catalyzed hydrolysis and associated sol−gel reaction used in electrodeposition procedures. (ii) SEM image and the corresponding EDS spectrum of carbon nanotubes deposited on a platinum foil electrode along with silica. (iii)

AFM height images of silica-coated nanotubes synthesized by electrochemical deposition of carbon nanotubes dispersed in the solution. (iv) Additional HRTEM images of nanotubes electrodeposited with Si. (v) SEM image and corresponding EDS spectrum of a control sample. (vi) High-resolution XPS spectra of purified single-walled carbon nanotubes. (vii) High-resolution XPS spectra of a control sample. (viii) High-resolution XPS spectra of silica-coated nanotubes. This material is available free of charge via the Internet at http://pubs.acs.org.

References and Notes

(1) Iijima, S. *Nature* **1991**, *354*, 56.

(2) Dresselhaus, M. S.; Dresselhaus, G.; Avouris, P. *Carbon Nanotubes: Synthesis, Structure, Properties, and Applications*; Springer-Verlag: Berlin, 2001.

(3) Baughman, R. H.; Zakhidov, A. A.; de Heer, W. A. *Science* **2002**, *297*, 787.

(4) Avouris, P. *Acc. Chem. Res.* **2002**, *35*, 1026.

(5) Bahr, J.; Tour, J. M. *J. Mater. Chem.* **2002**, *12*, 1952.

(6) Hirsch, A. *Angew. Chem., Int. Ed* **2002**, *41*, 1853.

(7) Chen, J.; Hamon, M. A.; Hu, H.; Chen, Y.; Rao, A. M.; Eklund, P. C.; Haddon, R. C. *Science* **1998**, *282*, 95.

(8) Banerjee, S.; Hemraj-Benny, T.; Wong, S. S. *Adv. Mater.* **2005**, *17*, 17.

(9) Wind, S.; Appenzeller, J.; Martel, R.; Derycke, V.; Avouris, P. *Appl. Phys. Lett.* **2002**, *80*, 3817.

(10) Postma, H. W. C.; Teepen, T.; Yao, Z.; Grifoni, M.; Dekker, C. *Science* **2001**, *293*, 76.

(11) Kong, J.; Franklin, N. R.; Zhou, C.; Chapline, M. G.; Peng, S.; Cho, K.; Dai, H. *Science* **2000**, *287*, 622.

(12) Bottini, M.; Tautz, L.; Huynh, H.; Monosov, E.; Bottini, N.; Dawson, M. I.; Bellucci, S.; Mustelin, T. *Chem. Commun.* **2005**, *6*, 758.

(13) Vast, L.; Philippin, G.; Destree, A.; Moreau, N.; Fonseca, A.; Nagy, J. B.; Delhalle, J.; Mekhalif, Z. *Nanotechnology* **2004**, *15*, 781.

(14) Velasco- Santos, C.; Martinez-Hernadez, A. L.; Lozada-Cassou, M.; Alvarez-Castillo, A.; Castano, V. M. *Nanotechnology* **2002**, *13*, 495.

(15) Aizawa, M.; Shaffer, M. S. P. *Chem. Phys. Lett.* **2003**, *368*, 121.

(16) Fan, W.; Gao, L. *Chem. Lett.* **2005**, *34*, 954.

(17) Wojdel, J. C.; Bromley, S. T. *J. Phys. Chem. B* **2005**, *109*, 1387.

(18) Seeger, T.; Köhler, T.; Frauenheim, T.; Grobert, N.; Rühle, M.; Terrones, M.; Seifert, G. *Chem. Commun.* **2002**, *1*, 34.

(19) Ning, J.; Zhang, J.; Pan, Y.; Guo, J. *J. Mater. Sci. Lett.* **2003**, *22*, 1019.

(20) Hongbing, Z.; Chan, Z.; Wenzhe, C.; Minquan, W. *Chem. Phys. Lett.* **2005**, *411*, 373.

(21) Gavalas, V. G.; Andrews, R.; Bhattacharyya, D.; Bachas, L. G. *Nano Lett.* **2001**, *1*, 719.

(22) Coradin, T.; Lopez, P. J. *ChemBioChem* **2003**, *4*, 251.

(23) Ikuno, T.; Katayama, M.; Kamada, K.; Honda, S.-i.; Lee, J.-G.; Mori, H.; Oura, K. *Jpn. J. Appl. Phys.* **2003**, *42*, L1356.

(24) Ikuno, T.; Katyama, M.; Lee, K.-Y.; Kuzuoka, T.; Lee, J-G.; Honda, S.-i.; Mori, H.; Oura, K. *Jpn. J. Appl. Phys.* **2004**, *43*, L987.

(25) Fu, Q.; Lu, C.; Liu, J. *Nano Lett.* **2002**, *2*, 329.

(26) Whitsitt, E. A.; Barron, A. R. *Nano Lett.* **2003**, *3*, 775.

(27) Whitsitt, E. A.; Moore, V. C.; Smalley, R. E.; Barron, A. R. *J. Mater. Chem.* **2005**, *15*, 4678.

(28) Colorado, R. J.; Barron, A. R. *J. Mater. Chem.* **2004**, *16*, 2692.

(29) Colorado, R. J.; Diosomito, M. E.; Barron, A. R. *Adv. Mater.* **2005**, *17*, 1634.

(30) Pender, M. J.; Sowards, L. S.; Hartgerink, J. D.; Stone, M. O.; Naik, R. J. *Nano Lett.* **2006**, *6*, 40.

(31) Berguiga, L.; Bellessa, J.; Vocanson, F.; Bernstein, E.; Plenet, J. C. *Opt. Mater.* **2006**, *28*, 167.

(32) Liu, Y.; Tang, J.; Chen, X.; Wang, R.; Pang, G. K. H.; Zhang, Y.; Xin, J. H. *Carbon* **2006**, *44*, 158.

(33) Seeger, T.; Redlich, P.; Grobert, N.; Terrones, M.; Walton, D. R. M.; Kroto, H. W.; Rühle, M. *Chem. Phys. Lett.* **2001**, *339*, 41.

(34) Chiang, I. W.; Brinson, B. E.; Huang, A. Y.; Willis, P. A.; Bronikowski, M. J.; Margrave, J. L.; Smalley, R. E.; Hauge, R. H. *J. Phys. Chem. B* **2001**, *105*, 8297.

(35) Park, T.-J.; Banerjee, S.; Hemraj-Benny, T.; Wong, S. S. *J. Mater. Chem.* **2006**, *16*, 141.

(36) Deepa, P. N.; Kanungo, M.; Claycomb, G.; Sherwood, P. M. A.; Collinson, M. M. *Anal. Chem.* **2003**, *75*, 5399.

(37) Shacham, R.; Anvir, D.; Mandler, D. *Adv. Mater.* **1999**, *11*, 384.

(38) Bard, A. J.; Faulkner, I. R. *Electrochemical Methods. Fundamentals and Applications*; Wiley: New York, 1980.

(39) Bockris, J. O. M.; Khan, S. U. M. *Surface Electrochemistry*; Plenum: New York, 1993.

(40) Aldykiewicz, A. J., Jr.; Davenport, A. J.; Isaacs, H. S. *J. Electrochem. Soc.* **1996**, *143*, 147.

(41) Kuhn, A. T.; Chan, C. Y. *J. Appl. Electrochem.* **1983**, *13*, 189.

(42) Li, J.-L.; Kudin, K.; McAllister, M. J.; Prudhomme, R. K.; Aksay, I. A.; Car, R. *Phys. Rev. Lett.* **2006**, *96*, 176101.

(43) Iler, R. K. *The Chemistry of Silica*; Wiley: New York, 1979.

(44) Brinker, C. J.; Frye, G. C.; Hurd, A. J.; Ashley, C. S. *Thin Solid Films* **1991**, *201*, 97.

(45) Okpalugo, T. I. T.; Papakonstantinou, P.; Murphy, H.; McLaughlin, J.; Brown, N. M. D. *Carbon* **2005**, *43*, 153.

(46) Martinez, M. T.; Callejas, M. A.; Benito, A. M.; Cochet, M.; Seeger, T.; Anson, A.; Schreiber, J.; Gordon, C.; Marhic, C.; Chauvet, O.; Fierro, J. L. G.; Maser, W. K. *Carbon* **2003**, *41*, 2247.

(47) Bahr, J. L.; Tour, J. M. *Chem. Mater.* **2001**, *13*, 3823.

(48) Tour, J. M.; Dyke, C. A. *Chem. Eur. J.* **2004**, *10*, 812.

(49) Sen, R.; Rickard, S. M.; Itkis, M. E.; Haddon, R. C. *Chem. Mater.* **2003**, *15*, 4723.

(50) Krupke, R.; Hennrich, F.; Hampe, O.; Kappes, M. M. *J. Phys. Chem. B* **2003**, *107*, 5667.

(51) Huang, H.; Kajiura, H.; Maruyama, R.; Kadono, K.; Noda, K. *J. Phys. Chem. B* **2006**, *110*, 4686.

(52) Banerjee, S.; Wong, S. S. *J. Am. Chem. Soc.* **2004**, *126*, 2073.

(53) Dresselhaus, M. S.; Dresselhaus, G.; Saito, R. *Phys. Rep.* **2005**, *409*, 47.

(54) Dresselhaus, M. S.; Dresselhuas, G.; Jorio, A.; Souza Filho, A. G.; Pimenta, M. A.; Saito, R. *Acc. Chem. Res.* **2002**, *35*, 1070.

(55) Rao, A. M.; Richter, E.; Bandow, S.; Chase, B.; Eklund, P. C.; Williams, K. A.; Fang, S.; Subbaswamy, K. R.; Menon, M.; Thess, A.; Smalley, R. E.; Dresselhaus, G.; Dresselhaus, M. S. *Science* **1997**, *275*, 187.

(56) Yu, Z.; Brus, L. E. *J. Phys. Chem. B* **2001**, *105*, 1123.

(57) Brown, S. D. M.; Corio, P.; Marucci, A.; Pimenta, M. A.; Dresselhaus, M. S.; Dresselhaus, G. *Phys. Rev. B* **2000**, *61*, 7734.

(58) Chen, Z.; Ziegler, K. J.; Shaver, J.; Hauge, R. H.; Smalley, R. E. *J. Phys. Chem. B* **2006**, *110*, 11624.

(59) Dyke, C. A.; Tour, J. M. *J. Am. Chem. Soc.* **2003**, *125*, 1156.

(60) Osswald, S.; Flahaut, E.; Gogotsi, Y. *Chem. Mater.* **2006**, *18*, 1525.

(61) Bachilo, S. M.; Strano, M. S.; Kittrell, C.; Hauge, R. H.; Smalley, R. E.; Weisman, R. B. *Science* **2002**, *298*, 2361.

(62) Strano, M. S.; Doorn, S. K.; Haroz, E. H.; Kittrell, C.; Hauge, R. H.; Smalley, R. E. *Nano. Lett.* **2003**, *3*, 1091.

(63) Heller, D. A.; Barone, P. W.; Swanson, J. P.; Mayrhofer, R. M.; Strano, M. S. *J. Phys. Chem. B* **2004**, *108*, 6905.

(64) Karajanagi, S. S.; Yang, H.; Asuri, P.; Sellitto, E.; Dordick, J.; Kane, R. S. *Langmuir* **2006**, *22*, 1392.

(65) Hennrich, F.; Krupke, R.; Lebedkin, S.; Arnold, K.; Fischer, R.; Resasco, D. E.; Kappes, M. *J. Phys. Chem. B* **2005**, *109*, 10567.

(66) Strano, M. *J. Am. Chem. Soc.* **2003**, *125*, 16148.

(67) Krupke, R.; Hennrich, F.; Loehneysen, H. V.; Kappes, M. *Science* **2003**, *301*, 344.

(68) Chattopadhyay, D.; Galeska, I.; Papadimitrikopoulos, F. *J. Am. Chem. Soc.* **2003**, *125*, 3370.

(69) Strano, M. S.; Dyke, C. A.; Usrey, M. L.; Barone, P. W.; Allen, M. J.; Shan, H.; Kittrell, C.; Hauge, R. H.; Tour, J. M.; Smalley, R. E. *Science* **2003**, *301*, 1519.

(70) Banerjee, S.; Wong, S. S. *J. Phys. Chem. B* **2002**, *106*, 12144.

(71) Banerjee, S.; Wong, S. S. *Nano Lett.* **2004**, *4*, 1445.